Polyene-lipids: A new tool to image lipids

Lars Kuerschner[1], Christer S Ejsing[1], Kim Ekroos[2], Andrej Shevchenko[1], Kurt I Anderson[1] & Christoph Thiele[1]

Microscopy of lipids in living cells is currently hampered by a lack of adequate fluorescent tags. The most frequently used tags, NBD and BODIPY, strongly influence the properties of lipids, yielding analogs with quite different characteristics. Here, we introduce polyene-lipids containing five conjugated double bonds as a new type of lipid tag. Polyene-lipids exhibit a unique structural similarity to natural lipids, which results in minimal effects on the lipid properties. Analyzing membrane phase partitioning, an important biophysical and biological property of lipids, we demonstrated the superiority of polyene-lipids to both NBD- and BODIPY-tagged lipids. Cells readily take up various polyene-lipid precursors and generate the expected end products with no apparent disturbance by the tag. Applying two-photon excitation microscopy, we imaged the distribution of polyene-lipids in living mammalian cells. For the first time, ether lipids, important for the function of the brain, were successfully visualized.

Cells contain hundreds of different lipid species that form all biomembranes and store metabolic energy in fat deposits. In membranes, lipids separate into coexisting liquid phases, which drives membrane microdomain formation[1,2]. Microdomains regulate processes such as signal transduction[3], cellular transport and sorting[4]. However, progress in understanding lipid function in these as well as other cellular processes is hampered by methodological limitations, in particular the lack of adequate fluorescent lipid imaging techniques. For fluorescence microscopy of lipids, only a few anti-lipid antibodies and specific lipid-binding protein domains are available to serve as probes[5,6]. Therefore, scientists attach artificial fluorescent tags to lipid molecules to replace one of the fatty acid side chains. Lipids bearing the fluorescent groups NBD[7] or BODIPY[8] and also anthracene[9], pyrene[10] or diphenylhexatriene[11] are widely used to study metabolism and cellular transport[12]. These tags were introduced before the importance of lipid phase separation was appreciated, and only recently have the adverse effects of the commonly used tags on this property of lipids been recognized. Severe interference was shown *in vitro*[7,13], and the tags were termed 'ill-suited' to study lipid microdomains[14], questioning results obtained *in vivo* before.

Promising alternatives to established fluorescent labels are polyene lipids, linear hydrocarbons containing a conjugated double bond system that is uniquely similar to natural lipids. Parinaric acid[15], a natural polyene–fatty acid with four conjugated double bonds, was used for physicochemical studies[16] but not in microscopy because of its short-wavelength UV excitation and emission. However, conjugated systems with five double bonds, pentaenes, have absorption and emission spectra that are more red-shifted[17]. Recently, pentaene–carboxylic acids[17] and pentaene–dicarboxylic acids[18,19] were used for biophysical studies in liposomes. In this study, we explored the potential of polyenes to serve as a general tag for lipids in cell biology studies, showed their superior properties in mimicking natural lipids and demonstrated their application to fluorescence microscopy in living cells.

RESULTS

Synthesis of polyene lipids

To synthesize lipids containing the fluorescent pentaene tag, modifications were made to the previously reported synthesis procedure for pentaenoic acids[20]. To avoid the reduction-oxidation cycles of the previous synthesis that used Wadsworth-Horner-Emmons reactions, Wittig reactions were used to build the conjugated double bond system. Starting from hexadienal, two cycles of chain elongation gave the key precursor decatetraenal (**Fig. 1**). *Cis*-pentaene–fatty acids were formed by a further Wittig reaction. Here, a modified workup exploiting the insolubility of lithium salts of the fatty acids allows synthesis in multi-gram scale without the need of chromatographic separation. All-*trans*–fatty acids were made from *cis*-pentaene–fatty acids by iodine-catalyzed isomerization[20]. *Cis*-pentaene–fatty acids were coupled to sphingosine and sphingosylphosphorylcholine to give pentaene-ceramides and pentaene-sphingomyelin (pentaene-SM), respectively. The pentaene alkylglycerol, a precursor of ether lipids, was made from decatetraenal by Wittig reaction with a protected alkyl glycerol followed by deprotection.

Phase distribution of fluorescent SMs

Preferences for liquid-ordered versus liquid-disordered phases of polyene-SM and BODIPY-SM were studied using a liposome-based fluorescence quench assay[14,21,22]. First, we confirmed that quenching of both fluorophores occurred with comparable efficiency. We prepared liposomes consisting of only a liquid-disordered phase[22], that is, dioleoyl-phosphatidylcholine (dioleoyl-PC) with variable amounts of nitroxide-labeled quencher PC and a constant trace amount of the respective fluorescent lipid. Here, quenching
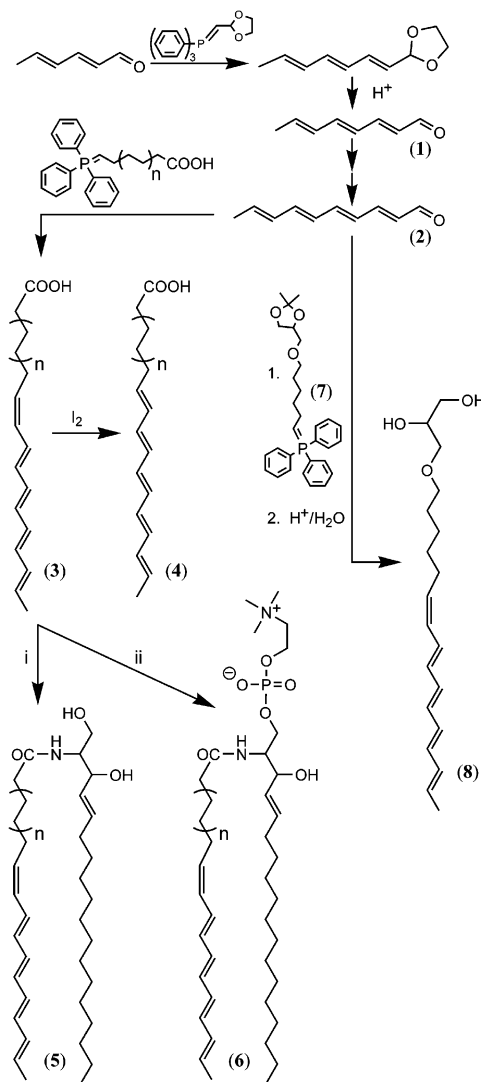
Figure 1 | A versatile procedure to introduce conjugated pentaene tags into lipids. The precursors, octatrienal (1) and decatetraenal (2), were constructed by repeated rounds of Wittig reactions. *Cis-* and *trans-*pentaene–fatty acids[20], (3) and (4), respectively, were obtained by a final Wittig reaction with a triphenylphosphonium salt of a ω-bromocarboxylic acid. The ω-9 double bond can be isomerized from *cis* (3) to *trans* (4) configuration. Fatty acids were activated and coupled to sphingosine or sphingosylphosphorylcholine to give pentaene-ceramide (5) or pentaene-SM (6), respectively. A Wittig reagent derived from a protected sn-1-O-alkylglycerol (7) couples to aldehyde (2) to give pentaene-alkylglycerol (8) after deprotection. Note that molecules (3) and (4) are the c and t 16:5–fatty acids, respectively, when N = 1 and c and t 18:5–fatty acids when N = 2.

Figure 2 | Analysis of phase partitioning of fluorescent SM analogs. (**a,b**) For a fluorescence quenching assay, series of liposomes comprising a liquid-disordered phase only (**a**), or coexisting liquid-ordered and liquid-disordered phases (**b**) were prepared containing variable amounts of a quencher lipid, 1-palmitoyl-2-stearoyl-(12-DOXYL)-PC, and traces of the fluorescent SM analogue. The quencher lipid prefers the liquid-disordered (L-α) phase. Normalized fluorescence $(F/F_0)_{cor}$ is plotted as a function of the quencher concentration. Data are mean $\pm$ range, n = 2 for open symbols, or mean $\pm$ s.d., n = 4 for closed symbols. Error bars smaller than symbol size were omitted. Note the difference between polyene-SMs and BODIPY-SMs in **b**, suggesting a preference of polyene-SMs for the liquid-ordered (raft) phase. DOPC, dioleoylphosphatidycholine. (**c**) Partitioning of fluorescent SM analogs into detergent-resistant membranes (DRMs) of COS7 cells. Cells were incubated with NBD-, BODIPY-, or polyene-ceramide prior to detergent solubilization with Lubrol-WX on ice. DRMs were floated on a linear sucrose gradient and fractions were analyzed for cell-derived SMs by thin-layer chromatography (TLC). Plates were photographed under UV illumination to visualize fluorescent SMs, followed by sulfuric acid charring to visualize total SMs and PCs. DRMs are found in fractions 3–5, solubilized material in fractions 6–8.

depends only on the efficiency of the quench process and geometrical factors[21]. The observed steep decrease of fluorescence for both c18:5-SM and BODIPY-SM (**Fig. 2a**) indicated equal quenching efficiency for both probes (see Methods for side chain naming convention used in this article). Second, in a two-phase assay, the quencher PC, preferring the liquid-disordered phase, was added in increasing amounts to a correspondingly decreasing amount of natural SM, a fixed amount of cholesterol and trace amounts of fluorescent SM. If the fluorescent lipid prefers the liquid-ordered phase (low quencher concentration), fluorescence quenching is
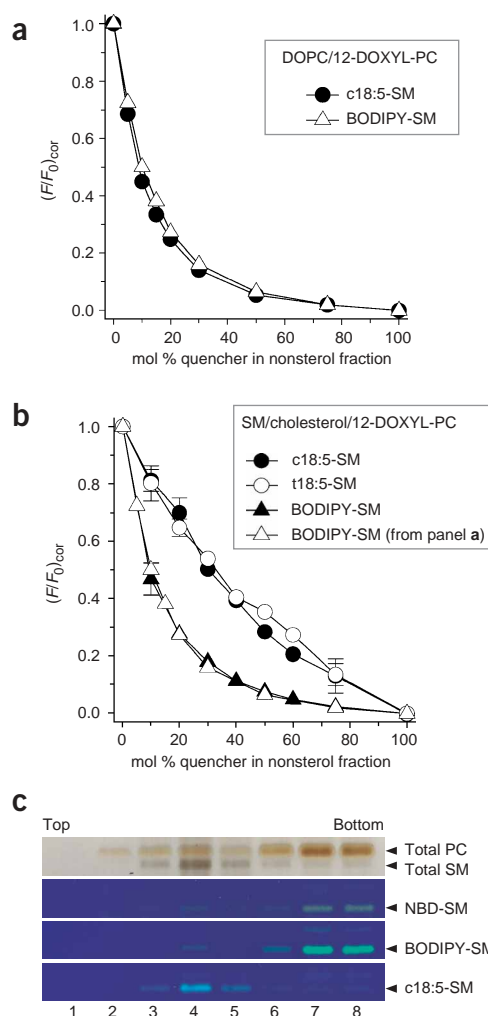
reduced relative to a lipid preferring the liquid-disordered phase (high quencher concentration). BODIPY-SM quenching was identical to that in the one-phase assay, indicating partitioning into the liquid-disordered phase (**Fig. 2b**). However, c18:5-SM yielded a much flatter curve, indicating partitioning into the liquid-ordered phase, and t18:5-SM displayed a similar curve with a slightly higher
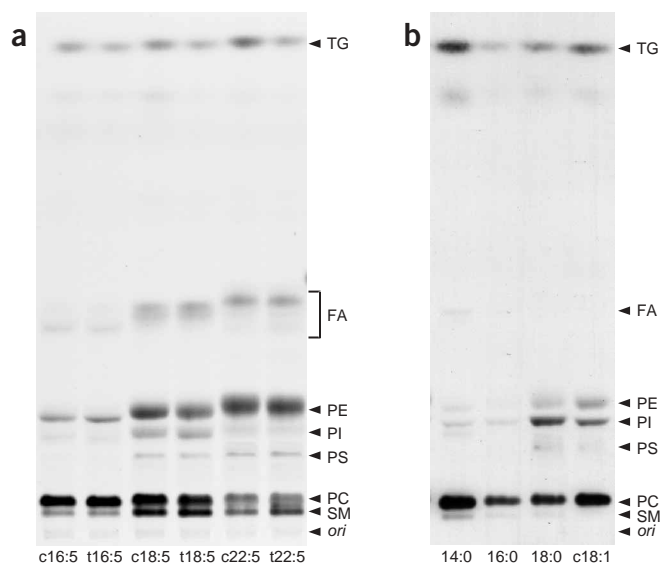
Figure 3 | Comparison of lipid metabolites of polyene-labeled or radioactive fatty acids in COS7 cells. Cells were incubated with 5 µM of the respective fatty acid for 20 h. Lipids were extracted and analyzed by TLC for fluorescent (**a**), or radioactive (**b**) metabolites, that were identified by comigrating lipid standards. Abbreviations are: CE, cholesterol ester; Cer, ceramide; DG, diglyceride; FA, fatty acid; *ori*, origin of application; PC, phosphatidylcholine; PE, phosphatidylethanolamine; PI, phosphatidylinositol; PS, phosphatidylserine; SM, sphingomyelin; TG, triglyceride.

fluorescent SM. Cells were lysed in the detergents Lubrol-WX[24] or Triton X-100[23] and then floated on a sucrose gradient. The floating Lubrol-WX–resistant membranes were strongly enriched in natural SM (**Fig. 2c**), cholesterol and glucosylceramide (data not shown). Polyene-SM floated like natural SM, but both NBD- and BODIPY-SM were found dissolved at the bottom of the gradient (**Fig. 2c**). Replacing Lubrol-WX with Triton X-100 gave the same result (data not shown). These experiments show that both natural SM and polyene-SM prefer the liquid-ordered phase, while both NBD- and BODIPY-SM fail to enter it.

Cellular metabolism of polyene lipids

We fed 5 µM concentrations of polyene–fatty acids to COS7 cells for 20 h and analyzed fluorescent metabolic products by TLC. We found that c/t16:5–fatty acids were incorporated mainly in PC, and longer ones (c/t18:5 and c/t22:5) were also incorporated into other phospholipids (**Fig. 3a**). Similar metabolism, apart from reduced SM labeling, was observed for radioactively-labeled natural fatty acids (**Fig. 3b**), demonstrating that polyene–fatty acids resemble natural fatty acids of comparable length with respect to utilization by the lipid biosynthetic enzymes.

Since polyene–fatty acids can be used in diverse cell types, we fed 50 µM t16:5–fatty acid to kidney epithelial cells (COS7, **Fig. 4a**), adipocytes (3T3-L1, **Fig. 4b**) and muscle cells (C2C12, **Fig. 4c**), all of which incorporated the polyene–fatty acid into various lipids. Different labeling times for different cell lines were necessary to incorporate sufficient polyene-lipid for high-quality imaging. High labeling selectivity, supporting unequivocal interpretation of imaging data, was achieved at lower concentrations for incubation times of a few hours. COS7 cells incubated with 3 µM t16:5–fatty acid for 2 h showed a prominent labeling of PC (**Fig. 4d**). When fed with c16:5-monoalkyl-1-glycerol, a polyene precursor for ether lipids, COS7 cells produced labeled ether lipids (**Fig. 4e**). Prominently-labeled classes were ether-PC and ether-PE, which are also known to contain the majority of natural ether lipids[25]. To label sphingolipids, we fed polyene-ceramide complexed to γ-cyclodextrin[26] at final concentrations of 0.15–10 µM for 2–4 h to COS7 cells, which resulted in uptake and conversion to polyene-SM (**Fig. 4f**). As a γ-cyclodextrin complex,
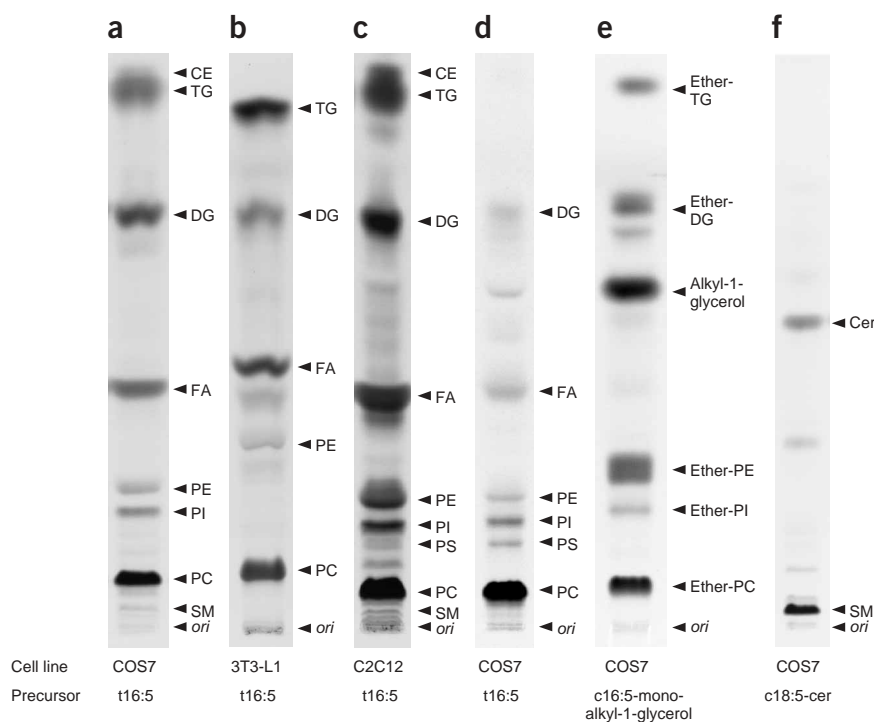
preference for the liquid-ordered phase at intermediate quencher concentrations (**Fig. 2b**). NBD-SM could not be studied because its hydrophilicity prevents sufficient incorporation into liposomes.

To corroborate these findings in a cellular system, we studied incorporation of fluorescent SMs into detergent-resistant membranes[23]. COS7 cells were fed NBD-, BODIPY- or polyene-ceramide, resulting in metabolic conversion to the respective

Figure 4 | Lipid metabolites of polyene–fatty acid in different cell types. (**a–c**) COS7 kidney epithelial cells (**a**), 3T3-L1 adipocytes (**b**), and C2C12 muscle cells (**c**) were incubated with 50 µM t16:5–fatty acid for 30 min (**a**), 15 min (**b**) or 1 h (**c**).(**d–f**) Lipid metabolites of different polyene lipid precursors in COS7 cells. Cells were incubated with 3 µM t16:5–fatty acid (**d**), c16:5-monoalkyl-1-glycerol (**e**) or c18:5-ceramide (**f**) for 2 h (**d,e**) or 4 h (**f**). Lipids were extracted and analyzed by TLC for fluorescent metabolites, which were identified by comigrating lipid standards. Abbreviations as in **Figure 3**.
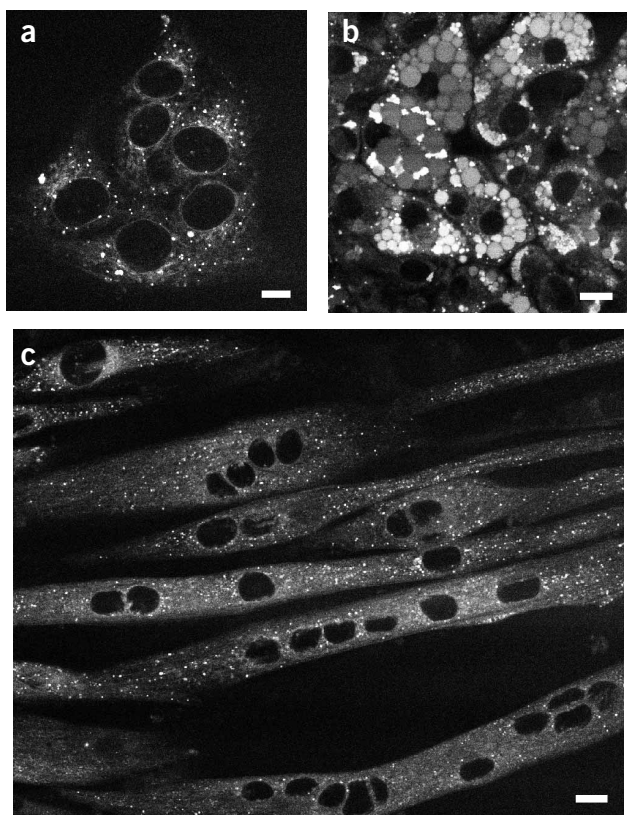
Figure 5 | Imaging of fluorescent polyene-lipids in various types of living mammalian cells. COS7 kidney epithelial cells (**a**), 3T3–L1 adipocytes (**b**) and C2C12 muscle cells (**c**) were grown with 50 μM t16:5–fatty acid for 30 min (**a**), 15 min (**b**), or 1 h (**c**). During this time fluorescent polyene-lipids (see **Fig. 4a**–**c**) were generated by cellular metabolism. Lipid distribution in living cells was imaged using two-photon-excitation microscopy. Bars, 10 μm.

Figure 6 | Localization of different lipid classes in living COS7 cells. COS7 cells transiently expressing mRFP1 targeted to the ER (upper panels), to peroxisomes (middle panels) or to the Golgi complex (lower panels) were grown for 2 h with 3 μM t16:5–fatty acid (upper panels), c16:5–monoalkyl-1-glycerol (middle panels) or c18:5–ceramide (lower panels). During this time mostly fluorescent PC (upper panels), various ether lipids (middle panels) and SM (lower panels) were generated by cellular metabolism (**Fig. 4d**–**f**). Two-photon–excited lipid distribution in living cells is shown in green, and mRFP1 signal is in red. Bars, 10 μm.

synthetic polyene-SM was also efficiently transferred to the cells (data not shown).

Saturated and unsaturated fatty acids display different preferences for the SN1 and SN2 positions in phospholipids. The preferences of polyene–fatty acids were analyzed by mass spectrometry. Lipid extracts of cells labeled with either t16:5– or c16:5–fatty acids were analyzed by precursor ion scanning for t/c16:5–containing species. Major species found were PCs containing 14:0–, 16:0–, 16:1– and 18:1–fatty acids and 16:0-ether–PC (**Supplementary Fig. 1** and **Supplementary Table 1** online). Analysis for positional preference[27] showed both t16:5– and c16:5–fatty acids predominantly at SN2 positions when combined with 14:0–, 16:0– and 18:1–fatty acids. In combination with palmitoleic acid, t16:5–fatty acid was preferentially located at the SN1 position, but c16:5–fatty acid was equally distributed (**Supplementary Table 1** online). Taking into account the relative amounts of labeled species, the majority of both 16:5–fatty acids was found at the SN2 position. Further fatty acid profiling showed that there was no metabolism of 16:5– to 16:4– or 18:5–fatty acids (data not shown). To detect effects of c/t16:5–fatty acids on unlabeled phospholipids, precursor ion scans for lipids containing 16:0–, 16:1–, 18:0–, 18:1–, 18:2–, 20:4– and 22:5–fatty acids were performed. No relevant differences between control cells and labeled cells were found (data not shown). Quantitative analysis revealed that labeling with 3 μM
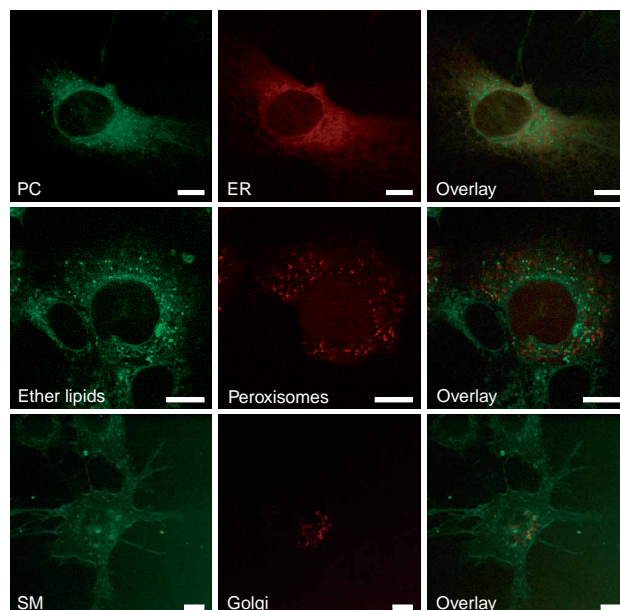
fatty acid for several hours or with 50 μM fatty acid for several minutes resulted in labeling of 0.5–2% of the total of the respective lipid class (data not shown), which seems unlikely to severely perturb membrane organization. Therefore, we used these concentrations for *in vivo* imaging of COS7 cells.

Imaging

For live-cell imaging of polyene-lipids, photodestruction of the polyene fluorophore was substantially reduced by using two-photon excitation[28], which allowed sequential acquisition of up to 50 images. The distribution of polyene-lipids in kidney epithelial cells (COS7, **Fig. 5a**), adipocytes (3T3-L1, **Fig. 5b**) and muscle cells (C2C12, **Fig. 5c**) was imaged, and we observed labeling of the nuclear envelope, lipid droplets and both endoplasmic and sarcoplasmic reticula. To accurately identify labeled cellular structures, we generated fusion proteins of mRFP1[29] as organellar markers. Colocalization studies of polyene-lipids and these markers in living COS7 cells were performed (**Fig. 6**). Labeling with 3 μM t16:5–fatty acid for 2 h generated mostly PC (**Fig. 4d**) and resulted in staining of nuclear envelope and endoplasmic reticulum (**Fig. 6**) plus lipid droplets and mitochondria (data not shown). Labeling inside the nucleus, shown for NBD– and BODIPY–fatty acids[30], was not observed. Labeling with polyene-alkylglycerol, which yielded fluorescent ether lipids (**Fig. 4e**), allowed their visualization in living cells for the first time. A distribution similar to that of PC was found (**Fig. 6**). Ether lipids did not accumulate in peroxisomes (**Fig. 6**), although the early steps of ether lipid biosynthesis occur there[25]. Labeling with

polyene-ceramide generated fluorescent SM (**Fig. 4f**), resulting in plasma membrane staining (**Fig. 6**) with little, if any, labeling of the Golgi complex, contrary to observations with NBD-ceramide[31] and BODIPY-ceramide[8].

DISCUSSION

Synthetic procedures developed in this study allow the incorporation of polyene tags into any lipid containing a straight hydrocarbon chain, as demonstrated for fatty acids and alkyl glycerol, which in turn give rise to fluorescent glycerophospholipids, neutral lipids, sphingolipids and ether lipids. This study focuses on pentaenes, but longer tags are also possible. Polyene-lipids with chain lengths of 12 carbon atoms and greater can be generated, and the position of the tag within the chain is adjustable according to the question under study. The first double bond (the one closest to the carboxy group) can be synthesized as *cis* or *trans*. The resulting geometrical differences resemble those between natural *cis*-unsaturated and saturated fatty acids, but this geometrical difference is much smaller for pentaenes than for the natural compounds (see **Supplementary Fig. 2** online), consistent with the similar properties of *cis*- and *trans*-pentaene–lipids observed in this study.

Although polyene-lipids and their natural counterparts possess very similar structural similarities, a word of caution should be added. The rigidity of the conjugated tag might influence its fate in biological systems[16], although this has not been apparent in our studies so far. Likewise, small changes in lipid molecular structure, such as the lack of a *trans* double bond in dihydroceramide can affect its functions[32]. For dihydroceramide, this is a consequence of a change in intramolecular hydrogen bonding between the amide and hydroxy groups[33]. For our fluorescent lipids, the relatively large distance between headgroups and the pentaene tag should minimize such effects. Generally, the final concentration of fluorescent lipids should be low to avoid changing the overall membrane properties.

Membrane organization into raft and non-raft domains plays an important role in many biological processes, including lipid localization and trafficking[34]. Therefore, fluorescent lipids should correspond to their natural counterparts regarding preference for the raft or non-raft phase. As we and others[7,13,14] show, NBD and BODIPY fluorophores interfere with the phase preference of natural SM and direct probes to the non-raft phase. This is a consequence of disrupted packing of NBD- and BODIPY-labeled lipids within the bilayer, due to the bulkiness and hydrophilicity of the fluorophore[5]. In contrast, polyene-SM is a lipid found preferentially in the raft-phase. Polyene side chains can be integrated into a liquid-ordered phase without disturbing the tight packing of hydrophobic chains[1,2]. The slightly higher preference for the raft phase of t18:5-SM compared to c18:5-SM can be explained by differences in geometry of the two fatty acids (**Supplementary Fig. 2** online).

We analyzed the metabolic fate of polyene lipid precursors upon application to living cells. As degradation of the polyene fluorophore via β-oxidation yields only non-fluorescent products, invisible in TLC and microscopic images, our analysis only accounts for those products that give a signal in microscopic imaging. Cells readily take up fluorescent precursors and convert them to the expected products with no apparent disturbance by the tag. Polyene-ceramide is converted to polyene-SM, and fluorescent ether lipids are generated from polyene-alkylglycerol. The labeling pattern of polyene–fatty acids follows that of radiolabeled natural fatty acids of the same length: shorter fatty acids show preference for incorporation into PC, longer ones have a wider distribution. The unequal degree of SM-labeling observed for fluorescent and radioactive fatty acids points to a preference of ceramide synthase for pentaene–fatty acids. This is unexpected because ceramide synthase normally prefers saturated fatty acids and it indicates that the kink in the geometry of *cis*-pentaene–fatty acids is not as pronounced as for a monounsaturated fatty acid, consistent with molecular modeling data (see **Supplementary Fig. 2** online). Labeling with higher concentrations of polyene–fatty acid resulted in accumulation of fluorescent intermediates of lipid biosynthesis, for example, free fatty acid and diglyceride, as well as labeled storage forms of lipids, such as triglyceride and cholesterol ester, suggesting saturation of the phospholipid biosynthesis. The results demonstrate that polyene-lipids are very similar to their natural counterparts in how they are used by the lipid biosynthetic enzymes, in contrast to the NBD– and BODIPY–fatty acids, which are poorly incorporated into cellular lipids[30].

Specific labeling of lipid classes or species is very useful. Occasionally, simple precursors express a preference for lipid classes, like the t16:5–fatty acid that incorporated preferentially into PC. Specificity is achieved by delivery of advanced precursors or lipid end products to the cell, such as ceramide and SM that were delivered as cyclodextrin complexes. Presumably, this will be a way to deliver other complex polyene-lipids, similar to pyrene-labeled lipids[26]. To achieve specific labeling of glycerophospholipids that are not covered by the present study, specific precursors such as polyene-lyso-PS and polyene-lyso-PE will be needed to generate polyene-PS and polyene-PE, respectively.

So far, steady state distribution of lipids has been characterized by subcellular fractionation and lipid analysis, often combined with electrospray mass spectrometry[35]. However, the fractionation procedure is limiting. Several organelles are difficult to obtain in sufficient amounts and purity, and subdomains of larger membranes with interesting functional specializations, for example, plasma membrane protrusions, cell-cell contact surfaces or ER exit sites, are virtually impossible to purify. In this study, real-time imaging using polyene lipids revealed a detailed view of lipid distribution. The striking staining of lipid droplets in adipocytes will enable us to characterize lipid flux into these storage organelles with high temporal and spatial resolution. Colocalization studies with fluorescent organelle markers, for the first time, show a distribution pattern of fluorescent SM and ceramide, which does not contradict results from fractionation studies. Polyene-sphingolipids do not accumulate at the Golgi apparatus but display a prominent plasma membrane staining, supporting the idea that SM is enriched at the plasma membrane at the expense of PC[36]. These findings differ from what has been observed for NBD-ceramide[31] and BODIPY-ceramide[8], which are markers for the Golgi apparatus. Both probes are trapped there by an unknown mechanism that at least for NBD-ceramide even functions in fixed cells[37]. Also, the localization of NBD– and BODIPY–fatty acids to the nucleus[30] is difficult to understand and cannot be confirmed for polyene–fatty acids used in our study. This accumulation may be caused by the cell's inability to esterify NBD– and BODIPY–fatty acids[30].

We provide the first images of the cellular distribution of ether lipids. This class of lipids, in which one hydrophobic side chain is attached via an ether instead of an ester linkage, is involved in

diverse physiological processes[25]. In humans, the lack of ether lipid results in fatal disease, and a corresponding mouse model shows male sterility, defects in myelination and optic nerve hypoplasia[38]. The cell biological background of these defects remains largely unclear. Therefore, polyene-tagged ether lipids represent a valuable tool to facilitate future studies of their cellular role.

Imaging of pentaenes is limited by the photophysical and photochemical properties of the fluorophore, in particular by the small quantum yield of one-tenth[17] and the sensitivity to photobleaching. Although quantum yield cannot be influenced, photobleaching was largely overcome by two-photon excitation and may be further improved by the total exclusion of oxygen during imaging[39]. Colocalization studies by multi-color imaging with two-photon excitation require the use of labels that are excited at one wavelength and separated on the emission side. mRFP1 fused to organelle targeting sequences for colocalization studies was satisfying for several markers, but weakly expressing constructs were not visualized with sufficient quality due to limitations of mRFP1[29]. Two-photon microscopy also enables imaging deep in tissue sections or intact organisms. In preliminary experiments, we imaged lipid uptake in the frequently used model organisms *Caenorhabditis elegans* and *Drosophila melanogaster*. The translucent zebrafish *Danio rerio*, an established model organism for developmental studies, is a candidate vertebrate for polyene lipid imaging.

METHODS

Fluorescent lipids. BODIPY-FL-C5-ceramide, BODIPY-FL-C5-SM and NBD-C6-ceramide were from Molecular Probes. Acyl or alkyl chains of polyene-lipids are denoted as follows: *cis/trans* configuration of the ω-9 double bond (c/t), followed by the number of carbon atoms and the number of double bonds, separated by a colon. All polyenes are pentaenes featuring conjugated double bonds at ω-9, ω-7, ω-5, ω-3 and ω-1 positions; the latter four in *trans* configuration.

Synthesis of polyene-lipids. See **Supplementary Methods** online.

Plasmids. See **Supplementary Methods** online.

Fluorescence quenching assays. The assay was performed according to the published procedure[14]. For a detailed description see **Supplementary Methods** online.

Cell culture and lipid delivery. COS7, 3T3-L1, and C2C12 cells were maintained in Dulbecco's modified Eagle's medium (DMEM) containing high glucose, GlutaMAX I and pyruvate (31966; Gibco) with 10% FCS. COS7 cells were transiently transfected using Cellfectin (Invitrogen). Confluent 3T3-L1 cells were differentiated to adipocytes with 500 mM 3-isobutyl-1-methylxanthine, 10 mM dexamethasone and 5 mg/ml insulin. After 3 d, 3-isobutyl-1-methylxanthine and dexamethasone were omitted. For up to 10 d, fresh medium was applied every 2 d until 90% of cells were differentiated. Confluent C2C12 cells were differentiated to myotubes in DMEM containing low glucose, L-glutamine and pyruvate (31885; Gibco) with 2% horse serum for 3 d. Sixteen hours prior to all experiments, cells were transferred to microscopy medium, DMEM with low glucose and pyruvate, free of glutamine and phenol red (11880; Gibco) and supplemented with 2 mM L-glutamine, 5% de-lipidated[40]

FCS. For microscopy cells were grown in number 1.5 glass bottom dishes (MatTek); for lipid analysis in 10 cm plates. Fatty acids or alkylglycerol at final concentration of up to 5 μM were added to microscopy medium by ethanolic injection. Polyene lipids or NBD- or BODIPY-tagged lipids at higher concentration were complexed to 1% delipidated BSA (Applichem) in HBSS as described[31]. Polyene-ceramide or polyene-SM was complexed to a twofold molar excess of γ-cyclodextrin (Applichem), dissolved in water by slowly injecting a few microliters of the lipid stock into vigorously stirring solution. After lyophilization, the complex was redissolved in microscopy medium and used immediately.

Detergent extraction and flotation. See **Supplementary Methods** online.

Lipid extraction. Cells were washed with PBS containing 1% delipidated BSA and collected by scraping. Cellular lipids were extracted as described[41], but the aqueous phase was acidified to pH 3.5 with citric acid. When extracting ether lipids, the pH of the aqueous phase was kept neutral. Dried lipids were redissolved in chloroform/methanol 2:1 and stored under nitrogen at –20 °C.

TLC and detection of lipids. Lipid samples were separated on silica TLC plates (Merck). After running two-thirds of the separation distance in chloroform/ethanol/water/triethylamine 35:40:9:35 (ref. 42), the plates were dried and subsequently separated in isohexane/ethylacetate 5:1 for the full distance. Digital images of TLC plates with fluorescent lipid samples were taken under UV illumination (312 nm) with a Canon D60 camera, converted to grayscale and inverted using Adobe Photoshop 6.0. Total lipids were detected by charring with sulfuric acid. Bands were identified by comparison with lipid standards.

Mass Spectrometry. Multiple precursor ion scanning was performed as previously described[43] on a QSTAR Pulsar i quadrupole time-of-flight mass spectrometer (MDS Sciex) with a nanoelectrospray ion source (Proxeon Biosystems). Prior to analysis, samples were diluted five- to tenfold in chloroform/methanol 1:2 containing 5 mM ammonium acetate. For head group scanning analysis the characteristic fragment ion of PC, m/z 184.1, was selected for detection of PCs and SMs in positive ion mode. Fragment ion of m/z 264.3 was selected for detection of ceramides in positive ion mode. For fatty acid scanning analysis in negative ion mode, precursor ion spectra were simultaneously acquired for 30 acyl anion fragments of fatty acid moieties, including those of polyene-fatty acids. Collision energy was set to 40 eV in positive and negative ion mode. Spectra were interpreted using prototype Lipid Profiler software (MDS Sciex)[27]. To monitor relative abundance of a molecular species, its peak area was related to the total of the respective lipid class. PC and SM species were quantitated together. The analysis was repeated three times and results were averaged.

Live cell imaging. Two-photon microscopy was performed using a Biorad Radiance 2100 MP setup attached to a Nikon Eclipse TE300 inverted microscope equipped with a Planapo 60× (1.2 NA). Pulsed excitation (pulse duration 200 fs, repetition rate 76 MHz, average power 600 mW) at 725 nm was provided by a 5 W Verdi/Mira laser (Coherent). Fluorescent images were

acquired using the non-descanned detectors. Long and short wavelengths were split using a 560DCXR beamsplitter (Chroma), and the longer ones were filtered with a D630/50m bandpass filter (Chroma). Images (852 × 852 pixels, 104 × 104 μm, recording time, 17 s per frame) were acquired using LaserSharp 2000 software (Biorad). Using this equipment, a lower limit of detection of pentaene lipids is at a concentration of 2 nmol/mg of cellular protein. All live cell imaging was done at 37 °C; the temperature of the specimen was controlled with a Tempcontrol 37–2 digital unit (Bachhoffer) and that of the objective, by an objective heater (Bioptechs). Images were processed using Adobe Photoshop 6.0.

Note: Supplementary information is available on the Nature Methods website.

1. Simons, K. & Ikonen, E. Functional rafts in cell membranes. *Nature* **387**, 569–572 (1997).
2. Brown, D.A. & London, E. Structure and origin of ordered lipid domains in biological membranes. *J. Membr. Biol.* **164**, 103–114 (1998).
3. Magee, T., Pirinen, N., Adler, J., Pagakis, S.N. & Parmryd, I. Lipid rafts: cell surface platforms for T cell signaling. *Biol. Res.* **35**, 127–131 (2002).
4. Holthuis, J.C., van Meer, G. & Huitema, K. Lipid microdomains, lipid translocation and the organization of intracellular membrane transport (Review). *Mol. Membr. Biol.* **20**, 231–241 (2003).
5. Maier, O., Oberle, V. & Hoekstra, D. Fluorescent lipid probes: some properties and applications (Review). *Chem. Phys. Lipids* **116**, 3–18 (2002).
6. Ishitsuka, R., Yamaji-Hasegawa, A., Makino, A., Hirabayashi, Y. & Kobayashi, T. A lipid-specific toxin reveals heterogeneity of sphingomyelin-containing membranes. *Biophys. J.* **86**, 296–307 (2004).
7. Chattopadhyay, A. Chemistry and biology of N-(7-nitrobenz-2-oxa-1,3-diazol-4-yl)-labeled lipids: fluorescent probes of biological and model membranes. *Chem. Phys. Lipids* **53**, 1–15 (1990).
8. Pagano, R.E., Martin, O.C., Kang, H.C. & Haugland, R.P. A novel fluorescent ceramide analogue for studying membrane traffic in animal cells: accumulation at the Golgi apparatus results in altered spectral properties of the sphingolipid precursor. *J. Cell Biol.* **113**, 1267–1279 (1991).
9. Stoffel, W. & Michaelis, G. Chemical syntheses of novel fluorescent-labelled fatty acids, phosphatidylcholines and cholesterol esters. *Hoppe-Seyler's Z. Physiol. Chem.* **357**, 7–19 (1976).
10. Somerharju, P. Pyrene-labeled lipids as tools in membrane biophysics and cell biology. *Chem. Phys. Lipids* **116**, 57–74 (2002).
11. Antes, P., Schwarzmann, G. & Sandhoff, K. Distribution and metabolism of fluorescent sphingosines and corresponding ceramides bearing the diphenylhexatrienyl (DPH) fluorophore in cultured human fibroblasts. *Eur. J. Cell Biol.* **59**, 27–36 (1992).
12. Pagano, R.E. & Sleight, R.G. Defining lipid transport pathways in animal cells. *Science* **229**, 1051–1057 (1985).
13. Kaiser, R.D & London, E. Determination of the depth of BODIPY probes in model membranes by parallax analysis of fluorescence quenching. *Biochim. Biophys. Acta* **1375**, 13–22 (1998).
14. Wang, T.Y. & Silvius, J.R. Different sphingolipids show differential partitioning into sphingolipid/cholesterol-rich domains in lipid bilayers. *Biophys. J.* **79**, 1478–1489 (2000).
15. Sklar, L.A., Hudson, B.S. & Simoni, R.D. Conjugated polyene fatty acids as membrane probes: preliminary characterization. *Proc. Natl. Acad. Sci. USA* **72**, 1649–1653 (1975).
16. Lentz, B.R. Use of fluorescent probes to monitor molecular order and motions within liposome bilayers. *Chem. Phys. Lipids* **64**, 99–116 (1993).
17. Mateo, C.R., Souto, A.A., Amat-Guerri, F. & Acuna, A.U. New fluorescent octadecapentaenoic acids as probes of lipid membranes and protein-lipid interactions. *Biophys. J.* **71**, 2177–2191 (1996).
18. Quesada, E., Acuna, A.U. & Amat-Guerri, F. New transmembrane polyene bolaamphiphiles as fluorescent probes in lipid bilayers. *Angew. Chem. Int. Edn. Engl.* **40**, 2095–2097 (2001).
19. Quesada, E., Acuna, A.U. & Amat-Guerri, F. Synthesis of carboxyl-tethered symmetric conjugated polyenes as fluorescent transmembrane probes of lipid bilayers. *Eur. J. Org. Chem.* **2003**, 1308–1318 (2003).
20. Souto, A.A., Ulises Acuna, A. & Amat-Guerri, F. A general and practical synthesis of linear conjugated pentaenoic acids. *Tetrahedr. Lett.* **35**, 5907–5910 (1994).
21. London, E. & Feigenson, G.W. Fluorescence quenching in model membranes. 1. Characterization of quenching caused by a spin-labeled phospholipid. *Biochemistry* **20**, 1932–1938 (1981).
22. Ahmed, S.N., Brown, D.A. & London, E. On the origin of sphingolipid/cholesterol-rich detergent-insoluble cell membranes: physiological concentrations of cholesterol and sphingolipid induce formation of a detergent-insoluble, liquid-ordered lipid phase in model membranes. *Biochemistry* **36**, 10944–10953 (1997).
23. Brown, D.A. & Rose, J.K. Sorting of GPI-Anchored proteins to glycolipid-enriched membrane subdomains during transport to the apical cell surface. *Cell* **68**, 533–544 (1992).
24. Roper, K., Corbeil, D. & Huttner, W.B. Retention of prominin in microvilli reveals distinct cholesterol-based lipid micro-domains in the apical plasma membrane. *Nat. Cell Biol.* **2**, 582–592 (2000).
25. Nagan, N. & Zoeller, R.A. Plasmalogens: biosynthesis and functions. *Prog. Lipid Res.* **40**, 199–229 (2001).
26. Tanhuanpaa, K. & Somerharju, P. Gamma-cyclodextrins greatly enhance translocation of hydrophobic fluorescent phospholipids from vesicles to cells in culture. Importance of molecular hydrophobicity in phospholipid trafficking studies. *J. Biol. Chem.* **274**, 35359–35366 (1999).
27. Ekroos, K. *et al.* Charting molecular composition of phosphatidylcholines by fatty acid scanning and ion trap MS3 fragmentation. *J. Lipid Res.* **44**, 2181–2192 (2003).
28. Denk, W., Strickler, J.H. & Webb, W.W. Two-photon laser scanning fluorescence microscopy. *Science* **248**, 73–76 (1990).
29. Campbell, R.E. *et al.* A monomeric red fluorescent protein. *Proc. Natl. Acad. Sci. USA* **99**, 7877–7882 (2002).
30. Huang, H., Starodub, O., McIntosh, A., Kier, A.B. & Schroeder, F. Liver fatty acid-binding protein targets fatty acids to the nucleus Real time confocal and multiphoton fluorescence imaging in living cells. *J. Biol. Chem.* **277**, 29139–29151 (2002).
31. Lipsky, N.G. & Pagano, R.E. A vital stain for the Golgi apparatus. *Science* **228**, 745–747 (1985).
32. Bielawska, A., Crane, H.M., Liotta, D., Obeid, L.M. & Hannun, Y.A. Selectivity of ceramide-mediated biology. Lack of activity of erythro-dihydroceramide. *J. Biol. Chem.* **268**, 26226–26232 (1993).
33. Li, L., Tang, X., Taylor, K.G., DuPre, D.B. & Yappert, M.C. Conformational characterization of ceramides by nuclear magnetic resonance spectroscopy. *Biophys. J.* **82**, 2067–2080 (2002).
34. Mukherjee, S. & Maxfield, F.R. Role of membrane organization and membrane domains in endocytic lipid trafficking. *Traffic* **1**, 203–211 (2000).
35. Brugger, B., Erben, G., Sandhoff, R., Wieland, F.T. & Lehmann, W.D. Quantitative analysis of biological membrane lipids at the low picomole level by nano-electrospray ionization tandem mass spectrometry. *Proc. Natl. Acad. Sci. USA* **94**, 2339–2344 (1997).
36. Sprong, H., van der Sluijs, P. & van Meer, G. How proteins move lipids and lipids move proteins. *Nat. Rev. Mol. Cell Biol.* **2**, 504–513 (2001).
37. Pagano, R.E., Sepanski, M.A. & Martin, O.C. Molecular trapping of a fluorescent ceramide analogue at the Golgi apparatus of fixed cells: Interaction with endogenous lipids provides a *trans*-Golgi marker for both light and electron microscopy. *J. Cell Biol.* **109**, 2067–2079 (1989).
38. Rodemer, C. *et al.* Inactivation of ether lipid biosynthesis causes male infertility, defects in eye development and optic nerve hypoplasia in mice. *Hum. Mol. Genet.* **12**, 1881–1895 (2003).
39. Tanhuanpaa, K., Virtanen, J. & Somerharju, P. Fluorescence imaging of pyrene-labeled lipids in living cells. *Biochim. Biophys. Acta* **1497**, 308–320 (2000).
40. Thiele, C., Hannah, M.J., Fahrenholz, F. & Huttner, W.B. Cholesterol binds to synaptophysin and is required for biogenesis of synaptic vesicles. *Nat. Cell Biol.* **2**, 42–49 (2000).
41. Bligh, E.G. & Dyer, W.J. A rapid method for total lipid extraction and purifiaction. *Can. J. Biochem. Physiol.* **37**, 911–917 (1959).
42. Dasgupta, S. & Hogan, E.L. Chromatographic resolution and quantitative assay of CNS tissue sphingoids and sphingolipids. *J. Lipid Res.* **42**, 301–308 (2001).
43. Ekroos, K., Chernushevich, I.V., Simons, K. & Shevchenko, A. Quantitative profiling of phospholipids by multiple precursor ion scanning on a hybrid quadrupole time-of-flight mass spectrometer. *Anal. Chem.* **74**, 941–949 (2002).